A variational approach to optical flow estimation of unsteady incompressible flows

Souvik Roy, Praveen Chandrashekar & A. S. Vasudeva Murthy

International Journal of Advances in Engineering Sciences and Applied Mathematics

ISSN 0975-0770
Volume 7
Number 3

Int J Adv Eng Sci Appl Math (2015)
7:149-167
DOI 10.1007/s12572-015-0147-9

Springer

Int J Adv Eng Sci Appl Math (July–September 2015) 7(3):149–167
DOI 10.1007/s12572-015-0147-9

IIT, Madras

A variational approach to optical flow estimation of unsteady incompressible flows

Souvik Roy[1] · **Praveen Chandrashekar**[1] · **A. S. Vasudeva Murthy**[1]

Published online: 23 September 2015

Abstract We consider optical flow estimation of flows with vorticity governed by 2D incompressible Euler and Navier–Stokes equations. A vorticity-streamfunction formulation and optimization techniques are used. We use Helmholtz decomposition of the velocity field and prove existence of an unique velocity and vorticity field for the linearized vorticity equations. Discontinuous galerkin finite elements are used to solve the vorticity equation for Euler's flow to efficiently track discontinuous vortices. Finally we test our method with two vortex flows governed by Euler and Navier–Stokes equations at high Reynolds number which support our theoretical results.

Keywords Euler · Navier–Stokes · Vorticity · Streamfunction · Discontinuous Galerkin · Optimization · Linearization · Helmholtz decomposition · Incompressible

Mathematics Subject Classification 76M

1 Introduction

Optical flow method is the estimation of 2D velocities of objects in successive image sequences that are in apparent motion. The estimation is based on the changes in spatio-temporal brightness pattern recorded in successive image sequences. Our motivation for the present study is the problem of tracking the motion of clouds from satellite image sequences. This in turn will help us in understanding the movement of rain bearing clouds during the monsoon over the Indian subcontinent. Previous work in this direction are [9–13]. However a major problem in applying OFM to fluid flow, leave alone cloud motion is that the connection between optical flow in the image plane and fluid flow in the 3D world is yet to be understood satisfactorily [7]. Given this state of affairs we propose to apply OFM to images that are generated synthetically by solving the 2D incompressible Stokes and Navier–Stokes equation. Our aim is to track movement of vortex structures generated by solving the 2D incompressible Stokes and Navier–Stokes equation. Previous work in this direction includes the Horn–Schunck algorithm which implements a constraint free first order regularization approach with a finite differencing scheme [1], estimating optical flow involving prior knowledge that the flow satisfies Stokes equation [3] and higher order regularization with incompressibility constraint coupled with mimetic finite differencing scheme [4].

It is well known [1] that tracking rigid body motion by OFM can be done satisfactorily using nonlinear least squares technique whereas it is inadequate for fluid flow [8]. This is because rigid body motion has features like geometric invariance where local features such as corners, contours etc are usually stable over time [28]. However for fluid images these features are difficult to define leave alone being stable. This is one of the main problems in understanding the connection between optical flow and fluid flow [20, 22–24]. To recover fluid-type motions, a number of approaches have been proposed to integrate the basic optical flow solution with fluid dynamics constraints,

✉ Souvik Roy
1roysouvik@gmail.com; souvik@math.tifrbng.res.in

Praveen Chandrashekar
praveen@math.tifrbng.res.in

A. S. Vasudeva Murthy
vasu@math.tifrbng.res.in

[1] TIFR Center for Applicable Mathematics, Bangalore 560065, India

e.g., the continuity equation that describes the fluid property [24, 25] or the divergence-curl (div-curl) equation [24, 26] to describe spreading and rotation. Such a work has its importance in determining atmospheric motion vectors (AMV), tracking smoke propagation, determining motion of tidal waves using floating buoys. Since the basic idea in the variational approach is not to estimate locally and individually but to estimate non-locally by minimizing a suitable functional defined over the entire image section, we therefore prefer a variational approach. We are interested in tracking vortex based high-Reynolds number incompressible flows. In [35] we had used such a variational approach by minimizing a functional with data obtained at a fixed time t. We found out that even though the method is efficient and recovers Stokes flow exactly, it fails to recover vortex structures for high Reynolds number flows. As a consequence, we formulate a minimization problem by penalizing the tracking or advection error over space as well as time. We use the vorticity-streamfunction formulation for the Euler and Navier–Stokes equations. This is because our main aim is to capture vortex structures and we can directly get the vorticity as an output rather than computing the curl of the velocity which could lead to numerical errors.

The paper is organised as follows. In Sect. 2 a variational formulation is presented. In Sect. 3 a first kind of modified variational formulation using linearized form of the Euler and Navier–Stokes is used. Existence and uniqueness of solutions is showed. In Sect. 4 continuous and discontinuous finite element formulations for the minimizing equations are presented. Section 5 deals with some numerical experiments for the modified variational problem. In Sects. 6 and 7 a second kind of modified variational formulation is discussed using linearized form of the Euler and Navier–Stokes along with some numerical results. In Sects. 8 and 9 the variational formulation as described in Sect. 2 is used and numerical tests are done with it. Finally in Sect. 10 the results are analyzed.

2 Variational formulation

To estimate fluid flow, passive scalars propagated by the flow are traced. Examples of such scalars are smoke and brightness patterns of dense rain-bearing clouds whose intensity remains constant atleast for a short time span. These scalars can be represented by a function $E : \Omega \times \mathbb{R}^+ \longrightarrow \mathbb{R}$ so that $E(x, y, t)$ for $(x, y) \in \Omega$ represents snapshots of the image of the scalars at various times $t \in \mathbb{R}^+$. Here Ω is a bounded convex subset of $\mathbb{R}^2$. We assume our image $E(x, y, t) \in W^{1,\infty}(\Omega)$, for each t and hence in $L^2(\Omega)$ (as Ω is bounded). The constant brightness assumption of the tracers gives us the optical flow equation

$$\frac{\partial E}{\partial t} + \widetilde{\mathbf{U}} \cdot \nabla E = 0 \tag{1}$$

where $\widetilde{\mathbf{U}}(\mathbf{x}, t)$ is the optical velocity i.e, the velocity of the fluid which propagates the scalars in the images. Estimating fluid motion of E is the inverse problem of determining $\widetilde{\mathbf{U}}$ from the image sequence represented by E. To estimate fluid flow, we need to include flow dynamics as constraints. We assume $\widetilde{\mathbf{U}}$ satisfies the 2D incompressible Euler (Navier–Stokes) equations i.e the vorticity $\omega = \nabla \times \widetilde{\mathbf{U}}$ satisfies

$$\begin{aligned} &\omega_t + \widetilde{\mathbf{U}} \cdot \nabla \omega = 0 \left(\frac{1}{Re} \Delta \omega\right), \quad (\mathbf{x}, t) \in \Omega \times (0, T] \\ &\omega(\mathbf{x}, 0) = \omega_0(\mathbf{x}), \quad \mathbf{x} \in \Omega \end{aligned} \tag{2}$$

where Re is the Reynolds number. We also impose the boundary condition

$$\omega = 0, \quad \mathbf{x} \in \partial\Omega_- (\partial\Omega \text{ for Navier-Stokes})$$

where $\partial\Omega_-$ is the inflow boundary

$$\partial\Omega_- = \{\mathbf{x} \in \partial\Omega : \widetilde{\mathbf{U}} \cdot n < 0\} \tag{3}$$

where n is the unit normal on the boundary of Ω. We assume that all vortex stay in the interior of the domain at all times $t \in [0, T]$. Again, as $\nabla \cdot \widetilde{\mathbf{U}} = 0$, $\exists\, \psi$: $\Omega \times \mathbb{R}^+ \longrightarrow \mathbb{R}$, called streamfunction, such that

$$\widetilde{\mathbf{U}}(\mathbf{x}, t) = \nabla^{\perp} \psi(\mathbf{x}, t).$$

Hence ψ is governed by

$$-\Delta \psi = \omega \quad \text{in } \Omega. \tag{4}$$

For solving (4), we impose the boundary condition

$$\frac{\partial \psi}{\partial n} = g(\mathbf{x}, t) \qquad \text{on } \partial\Omega \quad \forall t \in [0, T]. \tag{5}$$

For uniqueness, ψ is chosen to satisfy

$$\int_{\Omega} \psi = 0 \qquad \forall t \in [0, T]. \tag{6}$$

We assume $\omega_0 \in L^{\infty}(\Omega)$ and $g(\cdot, t) \in H^{-1/2}(\partial\Omega) \quad \forall t \in [0, T]$. Given E, our aim is to determine appropriate g and ω_0 so that (2), (3), (4), (5), (6) can be solved to determine $\widetilde{\mathbf{U}}$. Such a pair (g, ω_0) can be obtained by minimizing the functional

$$\begin{aligned} J(\psi(\omega_0, g), \omega_0, g) = &\frac{1}{2} \int_Q (E_t + \nabla^{\perp} \psi . \nabla E)^2 \\ &+ \frac{\alpha^2}{2} \int_0^T \int_{\partial\Omega} |g|^2 + \frac{\beta^2}{2} \int_{\Omega} |\omega_0|^2 \end{aligned} \tag{7}$$

where α and β are regularization parameters and $Q = (0, T) \times \Omega$. The minimization problem can be stated as

$$\min_{(\omega_0,g)} \quad \{J(\omega_0,g) : (2)-(6) \text{ is satisfied.}\} \tag{P}$$

We consider three different formulations. In the first case, a linearized version of (2) is considered where the total velocity is a perturbation of a known flow which is constant. The motivation for such an assumption originates from the Helmholtz decomposition of the velocity vector field. Since we are dealing with vortex based flows, our aim is to capture vortex structures well. So splitting up the velocity field into its translational and rotational part with known translational components enables us to capture vortex structures well. This is also demonstrated in the numerical examples. At the theoretical level, we also show existence of an unique velocity field which is very important from the computational perspective. In the second case, we again consider a linearized version of (2) where the total velocity is a perturbation of an unknown constant velocity. This in principle is the Helmholtz decomposition with both the translational and rotational part unknown. From the numerical test cases in Sect. 7, it can be seen that vortex properties are recovered well. Finally, we consider the general case when the total nonlinear velocity is unknown. Since there is no extra assumption on the properties on the velocity field, we are unable to show existence of an unique velocity field which leads to a not so good recovery of vortex structures. This is expected as the flow dynamics does not include rotational properties and without prior information of the boundary conditions and initial vorticity, it poses a major challenge in recovery of vortex based flows.

3 Formulation 1: Linearized flow

We assume

$$\widetilde{\mathbf{U}} = \mathbf{U}_0 + \mathbf{U}$$

where $\mathbf{U}_0$ is a known constant and $\mathbf{U}$ is assumed to be small relative to $\mathbf{U}_0$. Linearizing (2) about $\mathbf{U}_0$ and combining (4), (6) we get

$$\begin{aligned} &\omega_t + \mathbf{U}_0 \cdot \nabla\omega = 0\left(\frac{1}{Re}\Delta\omega\right), \quad (\mathbf{x},t) \in \Omega \times (0,T] \\ &\omega(\mathbf{x},0) = \omega_0(\mathbf{x}), \quad \mathbf{x} \in \Omega \end{aligned} \tag{8}$$

$$\begin{aligned} &-\Delta\psi = \omega, \quad \text{in } \Omega \\ &\frac{\partial\psi}{\partial n} = g, \quad \text{on } \partial\Omega \\ &\int_\Omega \psi = 0 \qquad \forall t \in [0,T] \end{aligned} \tag{9}$$

where $\mathbf{U} = \nabla^\perp\psi$ and $\omega = \nabla \times \mathbf{U}$. The boundary condition now becomes

$$\omega = 0, \quad \mathbf{x} \in \partial\Omega_- (\partial\Omega \text{ for Navier-Stokes}) \tag{10}$$

where $\partial\Omega_-$ is the inflow boundary given as

$$\partial\Omega_- = \{\mathbf{x} \in \partial\Omega : \mathbf{U}_0 \cdot n < 0\}$$

where n is the unit normal on the boundary of Ω.

Our aim is to determine $\mathbf{U}$, and hence the total velocity $\widetilde{\mathbf{U}}$, by minimizing the functional

$$\begin{aligned} J(g,\omega_0) = &\frac{1}{2}\int_Q (E_t + (\nabla^\perp\psi(g,\omega_0) + \mathbf{U}_0)\cdot\nabla E)^2 \\ &+ \frac{\alpha^2}{2}\int_0^T \int_{\partial\Omega} |g|^2 + \frac{\beta^2}{2}\int_\Omega |\omega_0|^2 \end{aligned} \tag{P$_1$}$$

subject to (8), (9) and (10).

3.1 Existence and uniqueness of minimizer

We want to show existence of an unique minimizer of (P$_1$). Before that we state some standard definitions and results.

3.2 Preliminaries

Let $(Z, \|\cdot\|_Z)$ be a Banach space.

Theorem 1 *Let $J : Z \to \mathbb{R} \cup \{-\infty, \infty\}$ be a convex functional on Z. If J is bounded from above in a neighbourhood of a point $U_0 \in Z$, then it is locally bounded i.e. each $U \in Z$ has a neighbourhood on which J is bounded.*

Definition 1 A functional J defined on Z is said to be **locally Lipschitz** if at each $U \in Z$ there exists a neighbourhood $N_\epsilon(U)$ and a constant $R(U)$ such that if $V, W \in N_\epsilon(U)$, then

$$|J(V) - J(W)| \le R\|V - W\|_Z$$

If this inequaltiy holds throughout a set $Y \subseteq Z$ with R independent of U then we say that J is **Lipschitz** on Y.

Theorem 2 *Let J be convex on Z. If J is bounded from above in a neighbourhood of one point of X, then J is locally Lipschitz in Z.*

Theorem 3 *Let J be convex on Z. If J is bounded from above in a neighbourhood of one point of Z, then J is continuous on Z.*

Theorems 1, 2, 3 and Definition 1 can be found in [27]. We use the following theorem from [2] to establish an unique global minimizer for (P).

Theorem 4 (Existence and uniqueness of global minimizer) *Let $J : Z \to \mathbb{R} \cup \{-\infty, \infty\}$ be a lower semi-continuous strictly convex functional. Also let J be coercive i.e.*

$$\lim_{\|U\|_Z \to +\infty} J(U) = \infty.$$

Let C be a closed and convex subset of Z. Then J has a unique global minimum over C.

We now verify conditions stated in Theorem (4) for the functional J in (P_1). Let $Z = L^2([0,T];H^{\frac{1}{2}}(\partial\Omega)) \times L^2(\Omega)$ with the norm $\|(g,\omega_0)\|_Z = \left(\int_0^T \int_{\partial\Omega}|g|^2 + \int_\Omega|\omega_0|^2\right)^{1/2}$.

Theorem 5 *The functional J given in (P_1) is strictly convex with respect to (ω_0, g).*

Before proving Thoerem 5 we show that (ψ,ω) given by (8) and (9) is linear in (ω_0, g).

Lemma 1 *(ψ,ω) given by (8) and (9) is linear in $(g,\omega_0) \in L^2([0,T];H^{\frac{1}{2}}(\partial\Omega)) \times L^2(\Omega)$.*

Proof Let (ψ_1,ω_1) and (ψ_2,ω_2) satisfy (8) and (9) for (g^1,ω_0^1) and $(g^2,\omega_0^2) \in L^2([0,T];H^{\frac{1}{2}}(\partial\Omega)) \times L^2(\Omega)$ respectively. Let us consider $\widetilde{\omega}_0 = \alpha\omega_0^1 + \beta\omega_0^2$ for $\alpha,\beta \in \mathbb{R}$. Then we see that $\widetilde{\omega} = \alpha\omega_1 + \beta\omega_2$ satisfy (8) for initial condition $\widetilde{\omega}_0$. Now let $\widetilde{\psi} = \alpha\psi_1 + \beta\psi_2$. Then we see that $\widetilde{\psi}$ satisfies

$$\begin{aligned} &-\Delta\widetilde{\psi} = \widetilde{\omega}, \quad \text{in } \Omega \\ &\frac{\partial\widetilde{\psi}}{\partial n} = \widetilde{g}, \quad \text{on } \partial\Omega \\ &\int_\Omega \widetilde{\psi} = 0 \qquad \forall t \in [0,T] \end{aligned} \tag{11}$$

where $\widetilde{g} = \alpha g^1 + \beta g^2$. This shows (ψ,ω) is linear in (g,ω_0). □

Proof (Proof of Theorem 5) Let $X_1 = (g^1,\omega_0^1)$ and $X_2 = (g^2,\omega_0^2)$. Then for $0<\lambda<1$, we have

$$\begin{aligned} &J(\lambda X_1 + (1-\lambda)X_2) \\ &= \frac{1}{2}\int_Q \left\{E_t + \left[\nabla^\perp\psi(\lambda X_1 + (1-\lambda)X_2) + \mathbf{U}_0\right]\cdot\nabla E\right\}^2 \\ &\quad + \frac{\alpha^2}{2}\int_0^T\int_{\partial\Omega}\left|\lambda g^1 + (1-\lambda)g^2\right|^2 + \frac{\beta^2}{2}\int_\Omega\left|\lambda\omega_0^1 + (1-\lambda)\omega_0^2\right|^2 \\ &= \frac{1}{2}\int_Q \left\{(E_t + \mathbf{U}_0\cdot\nabla E) + \left[\nabla^\perp\psi(\lambda X_1 + (1-\lambda)X_2)\right]\cdot\nabla E\right\}^2 \\ &\quad + \frac{\alpha^2}{2}\int_0^T\int_{\partial\Omega}\left|\lambda g^1 + (1-\lambda)g^2\right|^2 + \frac{\beta^2}{2}\int_\Omega\left|\lambda\omega_0^1 + (1-\lambda)\omega_0^2\right|^2 \\ &\le \frac{1}{2}\int_Q 2(E_t + \mathbf{U}_0\cdot\nabla E)^2 + \left(\left[\lambda\nabla^\perp\psi(X_1) + (1-\lambda)\nabla^\perp\psi(X_2)\right]\cdot\nabla E\right)^2 \\ &\quad + \frac{1}{2}\int_Q 2(E_t + \mathbf{U}_0\cdot\nabla E)\cdot\left(\left[\lambda\nabla^\perp\psi(X_1) + (1-\lambda)\nabla^\perp\psi(X_2)\right]\cdot\nabla E\right) \\ &\quad + \frac{\alpha^2}{2}\left(\lambda\int_0^T\int_{\partial\Omega}|g^1|^2 + (1-\lambda)\int_0^T\int_{\partial\Omega}|g^2|^2\right) \\ &\quad + \frac{\beta^2}{2}\left(\lambda\int_\Omega|\omega_0^1|^2 + (1-\lambda)\int_\Omega|\omega_0^2|^2\right) \\ &\qquad \text{(Using Lemma 1 and convexity of } L^2 \text{ norm)} \end{aligned} \tag{12}$$

Equality holds iff $X_1 = X_2$. So for $X_1 \neq X_2$, we have

$$J(\lambda X_1 + (1-\lambda)X_2) < \lambda J(X_1) + (1-\lambda)J(X_2), \qquad 0<\lambda<1$$

This shows J is strictly convex with respect to (ω_0, g).

Theorem 6 *The constraint set $C = \{\omega \in L^2([0,T];L^2(\Omega)) : \omega$ satisfies (8) and (10)$\}$ is given by the level set of a convex function.*

Proof For the vorticity equation in (8) corresponding to Euler's flow, there is an unique solution $\omega \in L^2([0,T];L^2(\Omega))$ and it can be given by $S(t)\omega_0$ where $(S(t))_{t\ge 0}$ is a C_0-semigroup of contractions in $L^2([0,T];L^2(\Omega))$ [32]. For the vorticity equation in (8) corresponding to Navier–Stokes flow, there exists an unique solution $\omega \in L^2([0,T];L^2(\Omega))$ and it can be given by $\widetilde{S}(t)\omega_0$ where $(\widetilde{S}(t))_{t\ge 0}$ is a C_0-semigroup of contractions in $L^2([0,T];L^2(\Omega))$ [33]. Both the solutions for Euler and Navier–Stokes equations represented by ω satisfy

$$\|\omega(.,t)\|_{L^2(\Omega)} \le \|\omega_0\|_{L^2(\Omega)} \tag{13}$$

by the boundedness of the operator S. Let

$$A : L^2(\Omega) \longrightarrow L^2([0,T];L^2(\Omega))$$

be defined as

$$A(\omega_0) = S(t)\omega_0 \ (\text{or}\widetilde{S}(t)\omega_0)$$

where ω satisfies (8). As $S(\widetilde{S})$ is a bounded linear bijection, A is a bounded linear bijection. Consider the function

$$F(\omega_0) = A(\omega_0) - \omega$$

where $\omega \in L^2([0,T];L^2(\Omega))$ and satisfies (8). This is a convex bijection and hence the constraint set (8) and (10) is given by

$$F(\omega_0) = 0$$

i.e. the level set of a convex function. □

Theorem 7 *The constraint set (9) is given by the level set of a convex function.*

Proof The constraint set (9) is given as

$$\begin{aligned} &-\Delta\psi(\mathbf{x},t) = \omega, \quad \mathbf{x}\in\Omega \\ &\frac{\partial\psi}{\partial n} = g(\mathbf{x},t), \quad \text{in } \partial\Omega, \quad \forall t\in[0,T]. \\ &\int_\Omega \psi = 0 \qquad \forall t\in[0,T] \end{aligned} \tag{14}$$

We have

$$-\int_\Omega(\Delta\psi(\mathbf{x},t))\phi(\mathbf{x})dx = -\int_\Omega\omega(\mathbf{x},t)\phi(\mathbf{x})dx, \qquad \forall\phi\in H^1(\Omega) \tag{15}$$

Using integration by parts we obtain

$$\int_\Omega \nabla\psi(\mathbf{x},t)\cdot\nabla\phi(\mathbf{x}) - \int_{\partial\Omega} g(\mathbf{x},t)\phi(\mathbf{x}) = -\int_\Omega \omega(\mathbf{x},t)\phi(\mathbf{x}) \qquad \forall t\in[0,T] \tag{16}$$

Setting $\phi=\psi$, taking modulus on both sides of (16) and using Holder's inequality and Poincare–Wirtinger inequality gives

$$\|\psi\|_{H^1(\Omega)} \le \|g\|_{H^{\frac{1}{2}}(\partial\Omega)} + \|\omega\|_{L^2(\Omega)} \tag{17}$$

which implies

$$\int_0^T \|\psi\|_{H^1(\Omega)} \le \int_0^T \|g\|_{H^{\frac{1}{2}}(\partial\Omega)} + \int_0^T \|\omega\|_{L^2(\Omega)} \tag{18}$$

where

$$\|g\|_{H^{\frac{1}{2}}(\partial\Omega)} = \int_{\partial\Omega} |g|^2$$

Let us consider the solution operator of (14)

$$B : L^2([0,T];H^1(\Omega)) \longrightarrow L^2([0,T];H^{\frac{1}{2}}(\partial\Omega))$$
$$\psi \longmapsto g$$

We now show that B^{-1} is a bounded linear bijection. For a fixed $\omega\in L^2([0,T];L^2(\Omega))$, given $g\in L^2([0,T];H^{\frac{1}{2}}(\partial\Omega))$ there exists an unique $\psi\in L^2([0,T];H^1(\Omega))$ such that ψ satisfies (14). This shows that B is a bijection. Also B^{-1} is convex for if ψ_1 and ψ_2 satisfy (14) for boundary data g_1 and g_2 respectively then $\lambda\psi_1+(1-\lambda)\psi_2$ is a solution of (14) for boundary data $\lambda g_1+(1-\lambda)g_2$. By (18), B^{-1} is bounded. Hence B^{-1} is a bounded linear bijection. Now consider the function

$$G(g) = B^{-1}(g) - \psi$$

for any fixed $\omega\in L^2([0,T];L^2(\Omega))$ where $\psi\in L^2([0,T];H^1(\Omega))$ and satisfies (14). This is a convex bijection and hence the constraint set (14) is given by

$$G(g) = 0$$

i.e. the level set of a convex function. □

So the set

$$C = \{(g,\omega_0)\in Z : F(\omega_0)=0, \quad G(g)=0\} \tag{19}$$

is a closed convex subset of Z. We now show that J is continuous and coercive.

Theorem 8 *The functional J given in* (P_1) *is continuous*

Proof We will use Theorem 3 to prove our statement. We assume

$$\|E\|_{W^{1,\infty}(Q)} \le M. \tag{20}$$

As $0\in Z$, we consider a neighbourhood of zero given as $N_1=\{(g,\omega_0) : \|(g,\omega_0)\|_Z<1\}$. Now

$$\begin{aligned}|J(g,\omega_0)| &= \frac{1}{2}\int_Q (E_t + (\nabla^\perp\psi(g,\omega_0)+\mathbf{U}_0).\nabla E)^2 \\ &\quad + \frac{\alpha^2}{2}\int_0^T\int_{\partial\Omega}|g|^2 + \frac{\beta^2}{2}\int_\Omega|\omega_0|^2 \\ &\le \frac{1}{2}\int_Q \Big(E_t^2 + (\nabla^\perp\psi(g,\omega_0)\cdot\nabla E)^2 \\ &\quad + 2E_t(\nabla^\perp\psi(g,\omega_0)\cdot\nabla E)\Big) + C_1\|(g,\omega_0)\|_Z^2\end{aligned}$$

Using Hölder's inequality and (20), (13) and (17) we get

$$\begin{aligned}|J(g,\omega_0)| &< \frac{3M}{2}\mu(Q) + M^2\|(g,\omega_0)\|_Z^2 + C_1\|(g,\omega_0)\|_Z^2 \\ &< \frac{3M}{2}\mu(Q) + M^2 + C_1 \\ &< \infty.\end{aligned}$$

where $\mu(Q)$ is the measure of Q. This gives us $J(U)$ is bounded above in N_1. As J is convex (by Theorem 5) it implies J is continuous for all $U\in Z$ (by Theorem 3). □

Theorem 9 *The functional J given in* (P_1) *is coercive for $\alpha>0$ and $\beta>0$.*

Proof From (P_1) we get

$$J(g,\omega_0) \ge \frac{\alpha^2}{2}\int_0^T\int_{\partial\Omega}|g|^2 + \frac{\beta^2}{2}\int_\Omega|\omega_0|^2$$

As $\alpha,\beta>0$, let $L=\min\{\alpha,\beta\}$. Then $L>0$. So we have

$$J(g,\omega_0) \ge Ł\left(\int_0^T\int_{\partial\Omega}|g|^2 + \int_\Omega|\omega_0|^2\right) = L\|(g,\omega_0)\|_Z^2$$

So if $\|(g,\omega_0)\|_Z\to\infty$ then $J(g,\omega)\to\infty$. Hence J is coercive.

J is a strictly convex continuous coercive functional on Z and the constraint set C given in (19) is convex. By Theorem 4, the convex minimization problem (7) has an unique global minimizer.

3.3 Optimization using Lagrange multipliers

In Sect. 3.1, we showed existence of an unique minimizer of J defined in (P_1). Now we determine the optimum solution. The functional J is to be minimized subject to PDE constraints. This is done by the use of Lagrange multipliers [15]. We first write down the weak forms of (8) and (9). Multiplying (8) with a test function $y\in H^1([0,T];L^2(\Omega))$, integrating by parts with respect to t and incorporating initial conditions for ω, we get

$$\int_Q (-\omega y_t + (\mathbf{U}_0 \cdot \nabla \omega) y) + \int_\Omega \omega(T) y(T) - \omega_0 y(0) = 0. \tag{21}$$

If we consider the Navier–Stokes equation then performing an integration by parts over Ω and using boundary conditions on ω, we get

$$\int_Q (-\omega y_t + (\mathbf{U}_0 \cdot \nabla \omega) y) + \int_\Omega \omega(T) y(T) - \omega_0 y(0) + \frac{1}{Re} \int_Q \nabla \omega \cdot \nabla y = 0. \tag{22}$$

Multiplying (9) with a test function $\phi \in L^2([0,T]; H_a^1(\Omega))$, integrating by parts over Ω, and using boundary conditions on ψ we get

$$\int_Q (\nabla \psi \cdot \nabla \phi - \omega \phi) - \int_0^T \int_{\partial\Omega} g \phi = 0. \tag{23}$$

Hence to determine the optimal solution, the auxillary functional can be written as

$$\begin{aligned} \widetilde{J}(y, \omega, \phi, \psi, g, \omega_0) &= J + \int_Q (-\omega y_t + (\mathbf{U}_0 \cdot \nabla \omega) y) + \int_\Omega \omega(T) y(T) - \omega_0 y(0) \\ &+ \int_Q (\nabla \psi \cdot \nabla \phi - \omega \phi) - \int_0^T \int_{\partial\Omega} g \phi \left(+ \frac{1}{Re} \int_Q \nabla \omega \cdot \nabla y \right) \end{aligned} \tag{24}$$

where y is the Lagrange Multiplier corresponding to the first constraint (8) and ϕ is the Lagrange Multiplier corresponding to the second constraint (14). Here $\omega, y \in L^2([0,T]; L^2(\Omega))$ and $\psi, \phi \in L^2([0,T]; H_a^1(\Omega))$ where

$$H_a^1(\Omega) = \left\{ \psi \in H^1(\Omega) : \int_\Omega \psi = 0 \right\}.$$

3.4 PDE's obtained after minimization of $\widetilde{J}$

Taking the Gateaux derivative of $\widetilde{J}$ in (24) wrt $y, \omega, \phi, \psi, g, \omega_0$, the standard optimality conditions [6] are

$$\frac{\partial \widetilde{J}}{\partial y} = 0, \frac{\partial \widetilde{J}}{\partial \omega} = 0, \frac{\partial \widetilde{J}}{\partial \phi} = 0, \frac{\partial \widetilde{J}}{\partial \psi} = 0, \frac{\partial \widetilde{J}}{\partial g} = 0, \frac{\partial \widetilde{J}}{\partial \omega_0} = 0. \tag{25}$$

The first and second equations in (25) gives the vorticity equation and its adjoint

$$\begin{aligned} &\omega_t + \mathbf{U}_0 \cdot \nabla \omega = 0 \left(\frac{1}{Re} \Delta \omega \right) \\ &\omega(\mathbf{x}, 0) = \omega_0(\mathbf{x}) \\ &\omega = 0, \quad \mathbf{x} \in \partial\Omega_-(\partial\Omega) \end{aligned} \tag{26}$$

$$\begin{aligned} &y_t + \mathbf{U}_0 \cdot \nabla y = 0 \left(-\frac{1}{Re} \Delta y \right) \\ &y(\mathbf{x}, T) = 0 \\ &y = 0 \quad \text{on } \partial\Omega \end{aligned} \tag{27}$$

The third and fourth equations in (25) gives the equation for streamfunction and its adjoint

$$\begin{aligned} -\Delta \psi &= \omega, \quad \mathbf{U} = \nabla^\perp \psi \\ \frac{\partial \psi}{\partial n} &= g \\ \int_\Omega \psi &= 0 \end{aligned} \tag{28}$$

$$\begin{aligned} \Delta \phi &= -\nabla E \cdot \nabla^\perp F \\ \frac{\partial \phi}{\partial n} &= -F \frac{\partial E}{\partial t} \\ \int_\Omega \phi &= 0 \end{aligned} \tag{29}$$

where $F = E_t + \widetilde{\mathbf{U}} \cdot \nabla E$. The fifth and sixth equations in (25) gives the optimality conditions

$$\alpha^2 g = \phi, \qquad \beta^2 \omega_0 = y(0) \tag{30}$$

4 Finite element method for problem ($\mathbf{P}_1$)

Equations (26), (27), (28), (29) and (30) are solved using space-time finite elements, considering time as the third dimension. The Eqs. (26) and (27) represent the forward vorticity equation and its backward adjoint equation. For Navier–Stokes flow, the solutions to the equations are smooth because of the presence of an extra diffusivity term on the right hand side. So continuous Galerkin finite elements are used. For Euler's flow, vorticity is non-smooth. Since our aim is to capture vortex structures well, we use discontinuous Galerkin method. The equations (28) and (29) represent the streamfunction equation and its adjoint equation which are elliptic in nature and hence they are solved using continuous Galerkin finite elements.

4.1 Discontinuous Galerkin formulation for vorticity equation for Euler's flow

Equations (26) and (27) are solved using the finite element method. Since we are interested in tracking discontinuous vortices, discontinuous Galerkin finite elements are used. It is an explicit method and hence there is no global matrix inversion. Also stability and energy conservation is maintained. The normal velocity $\mathbf{U} \cdot n$ is continuous across the element boundary and hence use of correct upwind flux is possible maintaining the stability [29, 30]. Let T_h be a

triangulation of domain Q and consider the space of piecewise polynomials

$$V_h^k = \{v \in L^2(Q) : V|_K \in \mathbb{P}_0 \quad \forall K \in T_h\} \tag{31}$$

where $\mathbb{P}_0(K)$ is the space of constant polynomials on K. The vorticity equation associated to Euler's flow given in (26) can be rewritten in conservative form as

$$\widetilde{\nabla} \cdot \omega B = 0 \tag{32}$$

where

$$\widetilde{\nabla} = \left(\frac{\partial}{\partial x}, \frac{\partial}{\partial y}, \frac{\partial}{\partial t}\right)$$

and

$$B = (u_0, v_0, 1)$$

Multiplying by a function $v \in L^2(Q)$ with $\text{supp}(v) = K$ and integrate by parts

$$\int_{\partial K} (B.n)\omega v - \int_K \omega (B.\nabla v) = 0$$

We consider the upwind flux to approximate the first term in the integral given by

$$H(\omega_+, \omega_-, n) = (B.n)^+ \omega_+ + (B.n)^- \omega_-$$

where

$$(B.n)^+ \omega_+ + (B.n)^- \omega_- = \begin{cases} (B.n)\omega_+ & \text{if } (B.n) \geq 0 \\ (B.n)\omega_- & \text{if } (B.n) < 0 \end{cases}$$

Then the DG scheme in K is given as

$$\int_{\partial K} H(\omega_+^h, \omega_-^h, n) v^h - \int_K \omega^h (B.\nabla v^h) = 0$$

Incorporating the boundary conditions and adding the equations for all elements the discrete problem is to find $\omega^h \in V_h^k$ such that

$$\begin{aligned} &- \sum_{K \in \tau_h} \int_K \omega^h (B.\nabla v^h) + \sum_{e \in \Gamma_I} \int_e H(\omega_+^h, \omega_-^h, n)[\![v^h]\!] \\ &\quad + \int_{\Gamma_-} H(\omega_+^h, \omega_0, n) + \int_{\Gamma_+} ((B.n)\omega^h v^h) = 0 \\ &\forall v^h \in V_h^k \end{aligned} \tag{33}$$

where Γ_I represents the interior edges, Γ_- represents the inflow boundary given by

$$\Gamma_- = \{\mathbf{x} \in \partial\Omega : B.n(\mathbf{x}) < 0\} \tag{34}$$

and Γ_+ represents the outflow boundary. A detailed analysis of the scheme can be found in [31].

For the adjoint equation (27) the same DG formulation in (33) is used with ω^h replaced y^h, $B = (-u_0, -v_0, -1)$ and inflow boundary conditions as $y^h = 0$ using (34).

4.2 Continuous Galerkin formulation for vorticity equation for Navier–Stokes

For the vorticity equation associated to Navier–Stokes flow given in (26) let us define the continuous space

$$W_h^k = \{v \in C^0(Q) : V|_K \in \mathbb{P}_k \quad \forall K \in T_h\} \tag{35}$$

where $\mathbb{P}_k(K)$ is the space of polynomials of degree k on K. We choose $k = 1$ for our computations unless otherwise mentioned. The discrete problem is to find $\omega^h \in W_h^k$ such that

$$\begin{aligned} &\int_Q (-\omega^h v_t^h + (\mathbf{U}_0 \cdot \nabla \omega^h) v^h) + \frac{1}{Re} \int_Q \nabla \omega^h \cdot \nabla v^h \\ &\quad + \int_\Omega \left(\omega^h(T) v^h(T) - \omega_0 v^h(0)\right) = 0 \\ &\forall v^h \in W_h^k \end{aligned} \tag{36}$$

In a similar way, the discrete problem for the adjoint equation (27) is to find $y^h \in W_h^k$ such that

$$\begin{aligned} &\int_Q \left(y^h v_t^h - (\mathbf{U}_0 \cdot \nabla y^h) v^h - \frac{1}{Re} \int_Q \nabla y^h \cdot \nabla v^h + \int_\Omega y^h(0) v^h(0)\right) = 0 \\ &\forall v^h \in W_h^k \end{aligned} \tag{37}$$

with inflow boundary conditions $y^h = 0$.

4.3 Continuous Galerkin formulation for streamfunction equation

To solve the streamfunction equation given by (28), the problem can be stated as: given ω and g, we want to find $\psi \in L^2([0,T]; H_a^1(\Omega))$ such that

$$\begin{aligned} &\int_Q (\nabla \psi \cdot \nabla \bar{\psi} + \omega \bar{\psi}) - \int_0^T \int_{\partial\Omega} g \bar{\psi} = 0, \\ &\forall \bar{\psi} \in L^2([0,T]; H_a^1(\Omega)) \end{aligned} \tag{38}$$

As (38) is solved using finite element method, we need to determine a discrete approximation of the space $L^2([0,T]; H_a^1(\Omega))$. But this is difficult in practice. Also the compatibility condition

$$\int_Q \omega + \int_0^T \int_{\partial\Omega} g = 0$$

needs to be satisfied for existence of solutions. In order to overcome these issues, Lagrange multipliers are used to add the constraint (6)–(38). So the modified weak formulation is to find $(\psi, s) \in L^2([0,T]; H^1(\Omega)) \times \mathbb{R}$ such that

$$\begin{aligned} &\int_Q (\nabla \psi \cdot \nabla \bar{\psi} + \omega \bar{\psi}) + \int_Q \bar{s} \psi + \int_Q s \bar{\psi} - \int_0^T \int_{\partial\Omega} g \bar{\psi} = 0, \\ &\forall (\bar{\psi}, \bar{s}) \in L^2([0,T]; H^1(\Omega)) \times \mathbb{R} \end{aligned} \tag{39}$$

This determines a discrete approximation of the space $L^2([0,T];H^1(\Omega))$. Also the compatibility condition is automatically taken care of. So the discrete problem is to find $(\psi^h, s) \in W_h^k \times \mathbb{R}$ such that

$$\int_Q (\nabla\psi^h \cdot \nabla\bar{\psi}^h + \omega\bar{\psi}^h) + \int_Q \bar{s}\psi^h + \int_Q s\bar{\psi}^h - \int_0^T \int_{\partial\Omega} g\bar{\psi}^h = 0, \qquad \forall(\bar{\psi}^h, \bar{s}) \in W_h^k \times \mathbb{R} \tag{40}$$

A similar approach is used to solve the adjoint equation (29). After substituting the value of g and ω_0 from (30) in (33), (36) and (40), the discrete weak forms for the vorticity and streamfunction equations and their adjoints are combined and solved in a coupled way to obtain $\mathbf{U}$ and hence $\widetilde{\mathbf{U}}$. Next we describe the procedure to determine $E, E_t, \nabla E$.

4.4 Image data

Our aim is to generate a sequence of synthetic images E and try to recover the velocity given the information of the derivatives of E. For this purpose E is chosen whose analytic expression at $t = 0$ is

$$E_0(x,y) = E(x,y,0) = e^{-50[(x-1/2)^2+(y-1/2)^2]}.$$

To get E at all times, we solve the advection equation

$$\begin{aligned} &E_t + \mathbf{U}_e \cdot \nabla E = 0, \quad (\mathbf{x},t) \in \Omega \times (0,T] \\ &E(x,0) = E_0, \quad \text{in } \Omega \\ &E = 0, \quad \text{on } \Gamma_- \end{aligned} \tag{41}$$

where U_e represents the velocity obtained by solving incompressible Euler (43) or Navier–Stokes flow (44) using finite element method with appropriate boundary conditions and Γ_- is given by (34) with $B = (\mathbf{U}_e, 1)$. We want E and its derivatives to be differentiable. Hence the weak formulation can be stated as: find $E \in H_c^2(Q)$ such that

$$\int_Q (E_t + \mathbf{U}_e \cdot \nabla E)\widetilde{E} = 0$$

for all $\widetilde{E} \in H_0^2(Q)$ where

$$H_c^2(Q) = \{E \in H^2(Q) : E(x,0) = E_0 \text{ in } \Omega, E = 0 \text{ on } \Gamma_-\}.$$

The discrete problem is to find $E^h \in W_h^k \cap H_c^2(Q)$ such that

$$\int_Q (E_t^h + \mathbf{U}_e \cdot \nabla E^h)\widetilde{E}^h = 0 \tag{42}$$

for all $\widetilde{E}^h \in W_h^k \cap H_0^2(Q)$. Equation (42) is solved using space-time finite element method with quadratic elements. Thus the solution E^h can be written as

$$E^h = \sum_i E_i^h \phi_i$$

where ϕ_i are basis functions of W_h^k which are continuous and piecewise quadratic polynomials in each element. Hence the derivatives of E are evaluated by computing the derivatives of ϕ_i. The unsteady incompressible Euler equations can be written in vorticity-streamfunction form as

$$\begin{aligned} &\omega_t + \mathbf{U}_e \cdot \nabla\omega = 0, \qquad (\mathbf{x},t) \in \Omega \times (0,T] \\ &\omega(\mathbf{x},0) = \omega_0(\mathbf{x}), \qquad \mathbf{x} \in \Omega \\ &-\Delta\psi = \omega, \quad \text{in } \Omega \\ &\psi = g_1, \quad \text{on } \partial\Omega \end{aligned} \tag{43}$$

where $\mathbf{U}_e = \nabla^\perp\psi$ and $\omega = \nabla \times \mathbf{U}_e$. The unsteady incompressible Navier–Stokes equations can be written in vorticity-streamfunction form as

$$\begin{aligned} &\omega_t + \mathbf{U}_e \cdot \nabla\omega = \frac{1}{Re}\Delta\omega, \qquad (\mathbf{x},t) \in \Omega \times (0,T] \\ &\omega(\mathbf{x},0) = \omega_0(\mathbf{x}), \qquad \mathbf{x} \in \Omega \\ &\Delta\psi = \omega, \quad \text{in } \Omega \\ &\psi = \psi_b, \quad \text{on } \partial\Omega \end{aligned} \tag{44}$$

where $\mathbf{U}_e = \nabla^\perp\psi$, $\omega = \nabla \times \mathbf{U}_e$, Re is the Reynolds number and ψ_b is a prescribed boundary condition. In practice, derivatives of images will be computed using some finite differences which will introduce errors in the computed velocity.

4.5 Test vortex flows

Our domain is $Q = (0,T) \times \Omega$, where $\Omega = [0,1] \times [0,1]$. Two types of vortex flows are considered.

Vortex 1: The tangential velocity distribution for the initial condition for vorticity is prescribed between an outer radius $r = R_O$, and a core radius $r = R_C$. For radius greater than R_O the tangential velocity is set to be zero. The tangential velocity of the vortex is expressed as follows:

$$u_\theta(r) = \begin{cases} U_c \dfrac{r}{R_C} & r < R_C \\ Ar + \dfrac{B}{r} & R_C \le r \le R_O \end{cases} \tag{45}$$

where

$$A = \frac{U_C R_C}{R_O^2 - R_C^2}, B = \frac{U_C R_C R_O^2}{R_O^2 - R_C^2}$$

Then the initial vorticity is given by

$$\omega(x,y,0) = \begin{cases} 2A, & R_C \le r \le R_O \\ 2A_1, & r \le R_C \end{cases} \tag{V1}$$

where $A_1 = \frac{U_C}{R_C}$. Our computations are done with $R_O = 0.2$ and $R_C = 0.1$.

Vortex 2: A vortex patch whose initial condition is as follows:

$$\omega(x,y,0) = \begin{cases} -2, & 0.2 \le x \le 0.6, 0.1 \le y \le 0.4 \\ 2, & 0.2 \le x \le 0.6, 0.55 \le y \le 0.85 \\ 0 & \text{otherwise} \end{cases} \quad \text{(V2)}$$

On $\partial\Omega$, Dirichlet boundary condition $\mathbf{U}_e = (0.5, 0)$ is imposed. This is equivalent to Dirichlet boundary condition $\psi = -0.5y$.

4.6 Mesh

The computations are done using COMSOL Multiphysics. The domain Q is partitioned into tetrahedrons as shown in Fig. 1. The average mesh size is $h = 0.01$. There are 196365 triangles with 1640836 degrees of freedom.

Computations for Navier–Stokes flow are done with $Re = 1000$.

4.7 Solving equations (43) and (44)

To solve (43) and (44) using finite element method to determine $\mathbf{U}_e$, a similar kind of approach for the vorticity equations as described in Sects. 4.1 and 4.2 is used. For solving the streamfunction equation, the weak formulation is to find $\psi \in L^2([0,T]; H_b^1(\Omega))$ such that

$$\int_Q (\nabla\psi \cdot \nabla\bar{\psi} + \omega\bar{\psi}) - \int_0^T \int_{\partial\Omega} g\bar{\psi} = 0, \quad \forall\bar{\psi} \in L^2([0,T]; H_b^1(\Omega)) \quad (46)$$

where

$$H_b^1(\Omega) = \{\psi \in H^1(\Omega) : \psi = \psi_b \text{ on } \partial\Omega\}$$

So the discrete problem is to find $\psi^h \in W_h^k \cap H_b^1$ such that

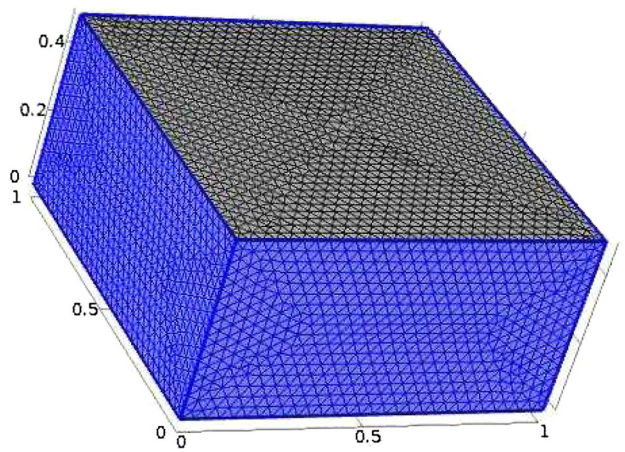

Fig. 1 3D mesh

$$\int_Q (\nabla\psi^h \cdot \nabla\bar{\psi}^h + \omega\bar{\psi}^h) = 0, \quad \forall\bar{\psi}^h \in W_h^k \cap H_0^1(\Omega) \quad (47)$$

The discrete weak forms as given in Sects. 4.1 and (47) for the vorticity equation and streamfunction equation are combined and solved in a coupled way to obtain $\mathbf{U}_e$. Finally the relative L^2 error in velocity is defined as

$$\text{Relative } L^2 \text{ error} = \frac{\|\mathbf{U}_e - \mathbf{U}_o\|}{\|\mathbf{U}_e\|} \quad (48)$$

and the advection error is defined as

$$\text{Advection Error} = \|E_t + \mathbf{U}_o \cdot \nabla E\| \quad (49)$$

where $\mathbf{U}_e$ is the exact velocity and $\mathbf{U}_o$ is the obtained velocity and the norm $\|\cdot\|$ is the usual L^2 norm in Q for vector functions.

5 Numerical examples

5.1 Advection of vortex 1 and vortex 2 under Euler's flow

The exact flow is given by solving (43) with initial vorticity given by (45) and (V2) and boundary condition for streamfunction given in Sect. 4.5. Figures 2 and 3 shows the velocity and vorticity plots at time $t = 0.5$. The figures show that the translational velocity, which is the constant velocity (0.5, 0), is well captured. Also the vortex movement is well recovered. Tables 1 and 2 shows the relative L^2 error and the advection error for various values of α and β. It has been numerically tested that for higher values of α and β of the order of 10^2 or greater gives bad results. This is because we are over-penalizing the initial vorticity and the boundary condition for the streamfunction leading to larger errors in the flow estimation. So for best results, we choose the value of α and β to be in the range of $[0.1, 10]$.

5.2 Advection of vortex 1 and vortex 2 under Navier–Stokes flow

The exact flow is given by solving (44) with initial vorticity given by (45) and (V2) and boundary condition for streamfunction given in Sect. 4.5. Figures 4 and 5 shows the velocity and vorticity plots at time $t = 0.5$. Again the figures show that the translational velocity, which is the constant velocity (0.5, 0), is well captured. Also the vortex movement is well recovered. We note the diffusivity of the vortex structures as is expected in Navier–Stokes flows. Tables 3 and 4 shows the relative L^2 error and the advection error for various values of α and β.

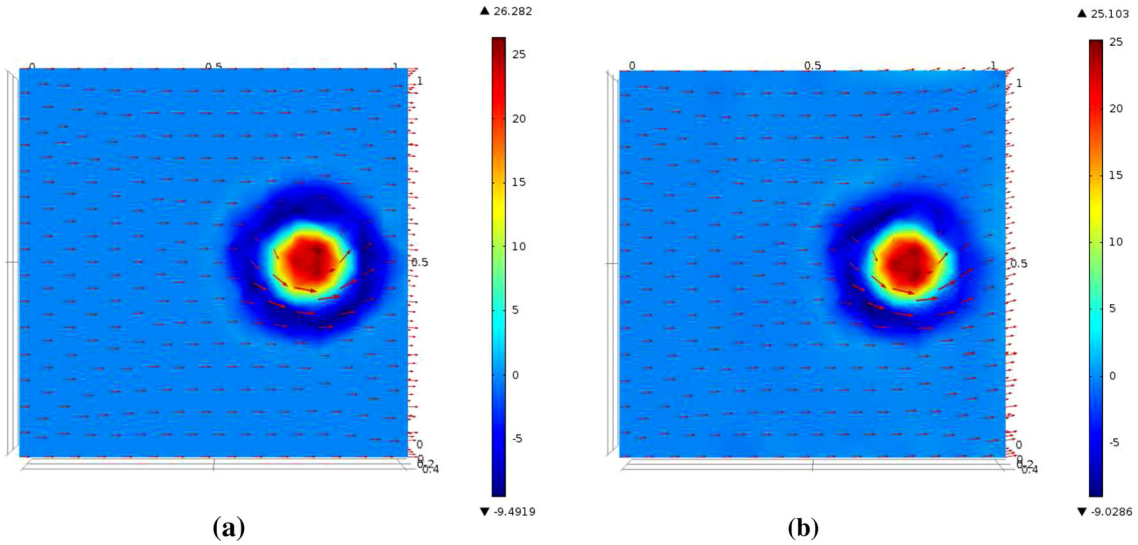

Fig. 2 Velocity and vorticity plots for vortex motion (45) under Euler's flow at $t = 0.5$ for $\alpha = \beta = 1$. **a** Exact, **b** recovered

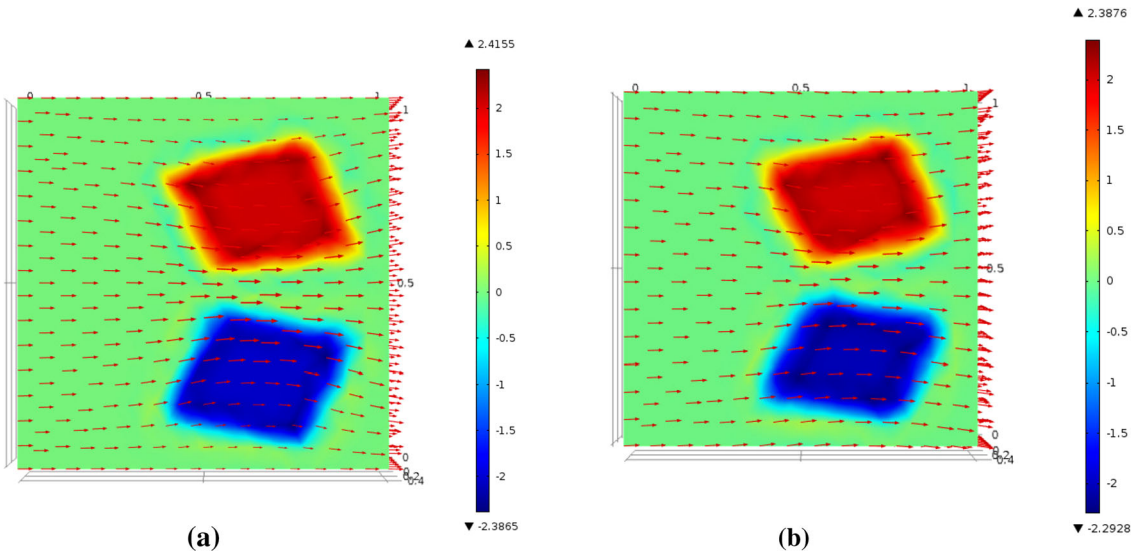

Fig. 3 Velocity and vorticity plots for vortex motion (V2) under Euler's flow at $t = 0.5$ for $\alpha = \beta = 1$. **a** Exact, **b** recovered

Table 1 Relative L^2 errors and advection errors for different values of α and β

α	β	Relative L^2 error	Advection error
0.01	0.01	2.5e−3	1.6e−4
1	1	2.8e−3	1.6e−4
10	10	2.7e−3	1.5e−4

Table 2 Relative L^2 errors and advection errors for different values of α and β

α	β	Relative L^2 error	Advection error
0.01	0.01	3.1e−3	1.1e−4
1	1	3.2e−3	1.1e−4
10	10	3.2e−3	1.1e−4

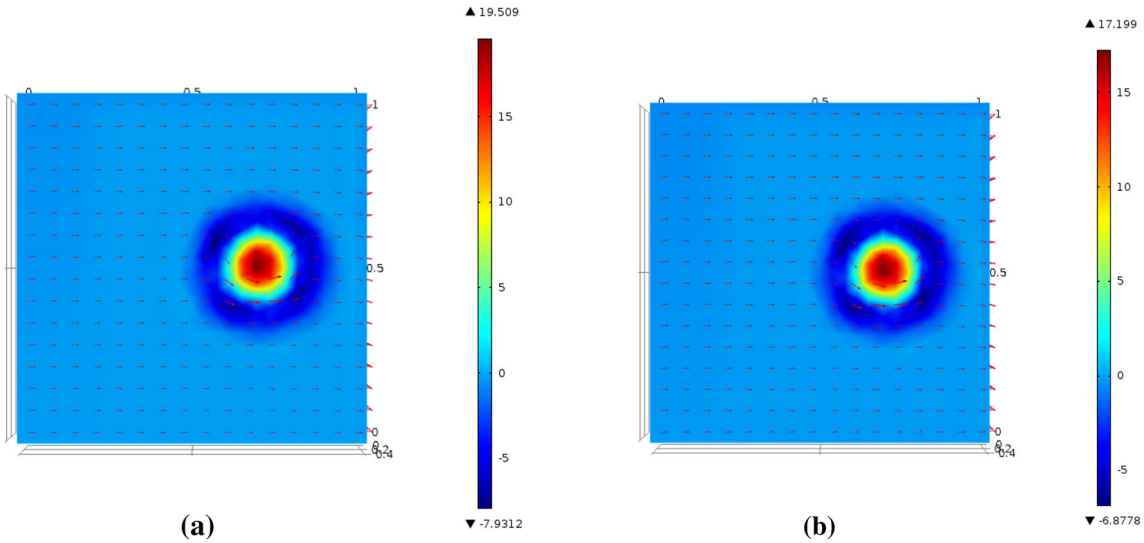

Fig. 4 Velocity and vorticity plots for vortex motion (45) under Navier–Stokes flow at $t = 0.5$ for $\alpha = \beta = 1$. **a** Exact, **b** recovered

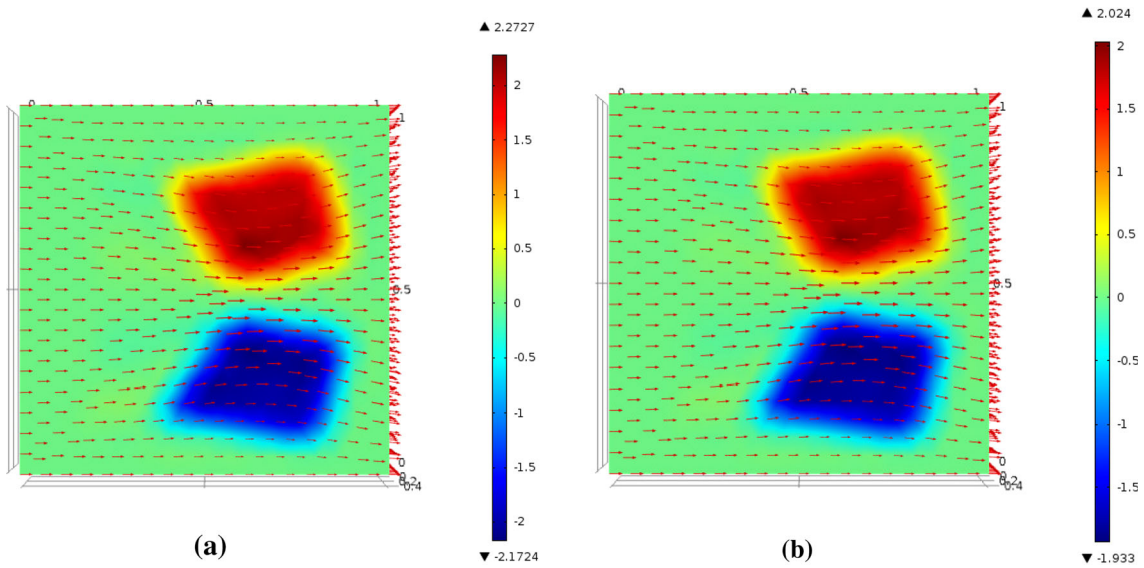

Fig. 5 Velocity and vorticity plots for vortex motion (V2) under Navier–Stokes flow at $t = 0.5$ for $\alpha = \beta = 1$. **a** Exact, **b** recovered

Table 3 Relative L^2 errors and advection errors for different values of α and β

α	β	Relative L^2 error	Advection error
0.01	0.01	5.1e−3	2.2e−4
1	1	5.2e−3	2.2e−4
10	10	5.1e−3	2.6e−4

Table 4 Relative L^2 errors and advection errors for different values of α and β

α	β	Relative L^2 error	Advection error
0.01	0.01	4.4e−3	2.7e−4
1	1	4.1e−3	2.5e−4
10	10	4.3e−3	2.4e−4

6 Formulation 2: Linearized flow

We now assume

$$\widetilde{\mathbf{U}} = \mathbf{U}_0 + \mathbf{U}$$

but now $\mathbf{U}_0$ is curl free, incompressible and unknown. Also $\mathbf{U}$ is assumed to be small relative to $\mathbf{U}_0$. This is the Helmholtz decomposition of $\widetilde{\mathbf{U}}$. Since $\mathbf{U}_0$ is unknown, we assume it is smooth and hence we add a regularization term to the functional J given in (P_1). Our aim is to determine $\mathbf{U}$ and hence the total velocity $\widetilde{\mathbf{U}}$ by minimizing

$$J_1(\psi, \omega_0, g, \mathbf{U}_0) = \frac{1}{2}\int_Q (E_t + \widetilde{\mathbf{U}}.\nabla E)^2 + \frac{\alpha^2}{2}\int_0^T \int_{\partial\Omega} |g|^2 + \frac{\beta^2}{2}\int_\Omega |w_0|^2 + \frac{\gamma^2}{2}\int_\Omega |\nabla \mathbf{U}_0|^2 \tag{50}$$

subject to the constraint set (8), (9) and (10).

6.1 Optimization using Lagrange multipliers

Using the weak forms for the vorticity and the stream-function equations given by (63) [or (64)] and (65) in Sect. 8.1, to determine the optimal solution, the auxillary functional can be written as

$$\begin{aligned}\widetilde{J}(y, \omega, \phi, \psi, \mathbf{U}_0, g, \omega_0) &= J_1 + \int_Q (-\omega y_t + (\mathbf{U}_0 \cdot \nabla\omega) y) + \int_\Omega \omega(T) y(T) - \omega_0 y(0) \\ &+ \int_Q (\nabla\psi \cdot \nabla\phi - \omega\phi) - \int_0^T \int_{\partial\Omega} g\phi \left(+ \frac{1}{Re}\int_Q \nabla\omega \cdot \nabla y \right)\end{aligned} \tag{51}$$

where y is the Lagrange multiplier corresponding to the first constraint set (8) and ϕ is the Lagrange multiplier corresponding to the second constraint set (14). Here $\omega, y \in L^2([0,T]; L^2(\Omega))$ and $\psi, \phi \in L^2([0,T]; H_a^1(\Omega))$ where

$$H_a^1(\Omega) = \left\{ \psi \in H^1(\Omega) : \int_\Omega \psi = 0 \right\}$$

6.2 PDE's obtained after minimization of $\widetilde{J}$

Taking the Gateaux derivative of $\widetilde{J}$ in (51) wrt $y, \omega, \phi, \psi, g, \omega_0$, the standard optimality conditions [6] are

$$\frac{\partial\widetilde{J}}{\partial y} = 0, \frac{\partial\widetilde{J}}{\partial\omega} = 0, \frac{\partial\widetilde{J}}{\partial\phi} = 0, \frac{\partial\widetilde{J}}{\partial\psi} = 0, \frac{\partial\widetilde{J}}{\partial\mathbf{U}_0} = 0, \frac{\partial\widetilde{J}}{\partial g} = 0, \frac{\partial\widetilde{J}}{\partial\omega_0} = 0 \tag{52}$$

The first and second equations in (52) gives the vorticity equation and its adjoint

$$\begin{aligned}&\omega_t + \mathbf{U}_0 \cdot \nabla\omega = 0\left(\frac{1}{Re}\Delta\omega\right) \\ &\omega(\mathbf{x}, 0) = \omega_0(\mathbf{x}) \\ &\omega = 0, \quad \mathbf{x} \in \partial\Omega_-(\partial\Omega)\end{aligned} \tag{53}$$

$$\begin{aligned}&y_t + \mathbf{U}_0 \cdot \nabla y = 0\left(-\frac{1}{Re}\Delta y\right) \\ &y(\mathbf{x}, T) = 0 \\ &y = 0 \quad \text{on } \partial\Omega\end{aligned} \tag{54}$$

The incompressibility of $\mathbf{U}_0$ is essential in obtaining (54). The third and fourth equations in (52) gives the equations for the streamfunction and its adjoint

$$\begin{aligned}-\Delta\psi &= \omega, \quad \mathbf{U} = \nabla^\perp\psi \\ \frac{\partial\psi}{\partial n} &= g \\ \int_\Omega \psi &= 0\end{aligned} \tag{55}$$

$$\begin{aligned}\Delta\phi &= -\nabla E.\nabla^\perp F \\ \frac{\partial\phi}{\partial n} &= -F\frac{\partial E}{\partial t} \\ \int_\Omega \phi &= 0\end{aligned} \tag{56}$$

The fifth equation in (52) gives the PDE satisfied by $\mathbf{U}_0$ with the boundary conditions

$$\begin{aligned}F\nabla E + y\nabla\omega - \gamma^2\Delta\mathbf{U}_0 &= 0 \\ \frac{\partial\mathbf{U}_0}{\partial n} &= 0\end{aligned} \tag{57}$$

where $F = E_t + \widetilde{\mathbf{U}} \cdot \nabla E$. The last two equations in (52) gives the optimality conditions

$$\alpha^2 g = \phi, \qquad \beta^2\omega_0 = y(0) \tag{58}$$

We again use a similar kind of computational approach as used in Sect. 4.

7 Numerical examples

7.1 Advection of vortex 1 and vortex 2 under Euler's flow

The exact flow is given by solving (43) with initial vorticity given by (45) and (V2) and boundary condition for streamfunction given in Sect. 4.5. Figures 6 and 7 shows the velocity and vorticity plots at time $t = 0.5$. As

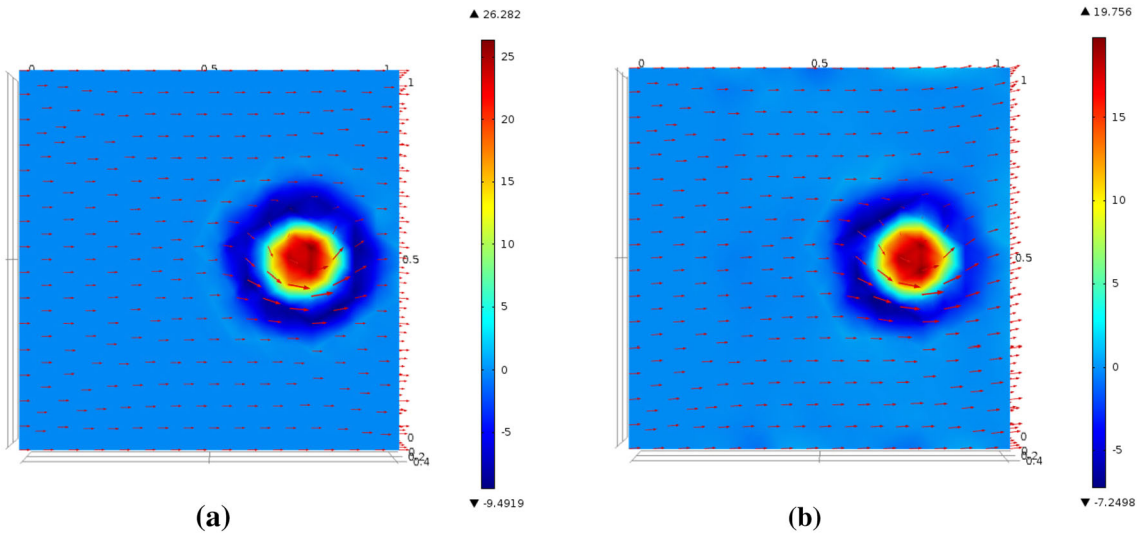

Fig. 6 Velocity and vorticity plots for vortex motion (45) under Euler's flow at $t = 0.5$ for $\alpha = \beta = \gamma = 1$. **a** Exact, **b** recovered

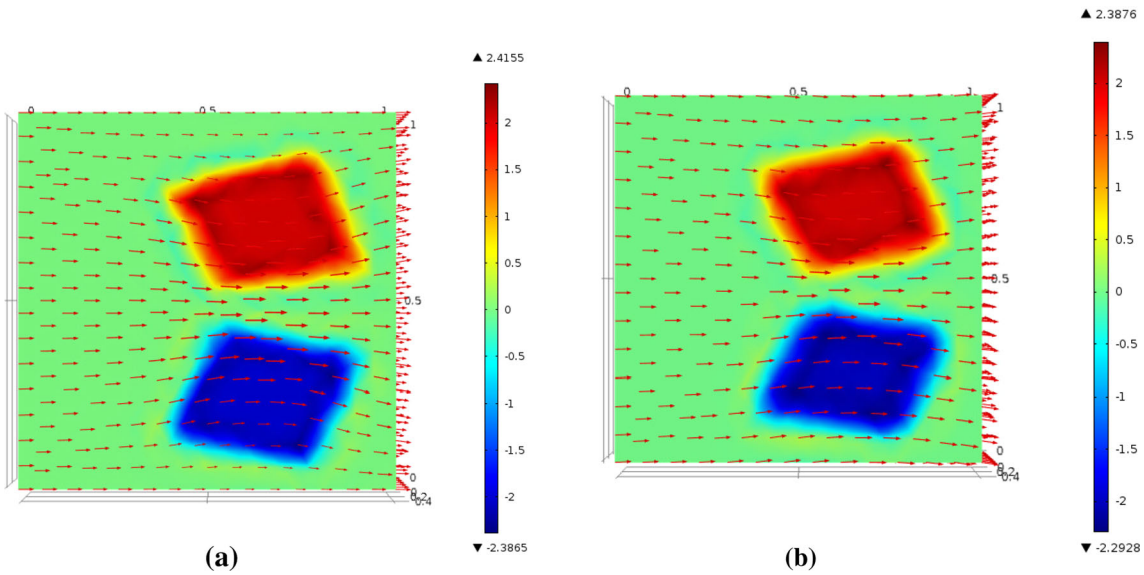

Fig. 7 Velocity and vorticity plots for vortex motion (V2) under Euler's flow at $t = 0.5$ for $\alpha = \beta = \gamma = 1$. **a** Exact, **b** recovered

Table 5 Relative L^2 errors and advection errors for different values of α, β and γ

α	β	γ	Relative L^2 error	Advection error
0.01	0.01	0.01	2.8e−3	1.3e−4
1	1	1	2.6e−3	1.4e−4
10	10	10	2.7e−3	1.3e−4

Table 6 Relative L^2 errors and advection errors for different values of α, β and γ

α	β	γ	Relative L^2 error	Advection error
0.01	0.01	0.01	3.5e−3	1.7e−4
1	1	1	3.4e−3	1.2e−4
10	10	10	3.1e−3	1.4e−4

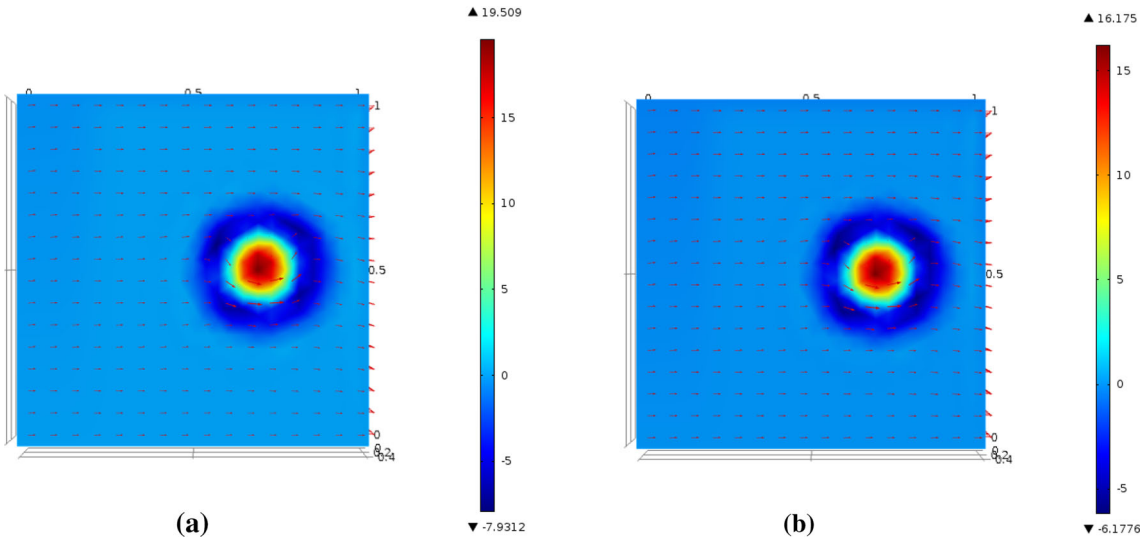

Fig. 8 Velocity and vorticity plots for vortex motion (45) under Navier–Stokes flow at $t = 0.5$ for $\alpha = \beta = \gamma = 1$. **a** Exact, **b** recovered

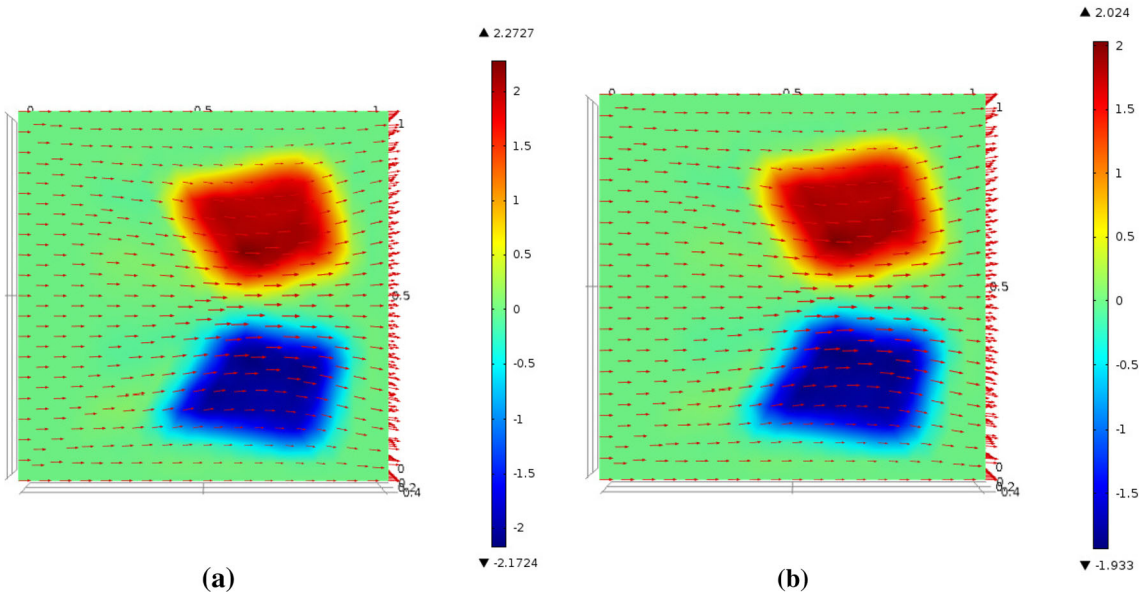

Fig. 9 Velocity and vorticity plots for vortex motion (V2) under Navier–Stokes flow at $t = 0.5$ for $\alpha = \beta = \gamma = 1$. **a** Exact, **b** recovered

Table 7 Relative L^2 errors and advection errors for different values of α, β and γ

α	β	γ	Relative L^2 error	Advection error
0.01	0.01	0.01	5.4e−3	2.8e−4
1	1	1	5.3e−3	2.4e−4
10	10	10	5.6e−3	2.7e−4

Table 8 Relative L^2 errors and advection errors for different values of α, β and γ

α	β	γ	Relative L^2 error	Advection error
0.01	0.01	0.01	4.3e−3	2.2e−4
1	1	1	4.4e−3	2.8e−4
10	10	10	4.6e−3	2.5e−4

in the test cases in Sect. 5.1, the translational velocity is well recovered. Also the vortex structures are well recovered. Tables 5 and 6 shows the relative L^2 error and the advection error for various values of α and β. As in the test cases in Sect. 5.1, the best results are obtained values of α and β in the range of $[0.1, 10]$. For the parameter γ we also use values in the range of $[0.1, 10]$ because higher values of γ lead to over-smoothening of the translational velocity field which is not desirable when we have discontinuous vortices.

7.2 Advection of vortex 1 and vortex 2 under Navier–Stokes flow

The exact flow is given by solving (44) with initial vorticity given by (45) and (V2) and boundary condition for streamfunction given in Sect. 4.5. Figures 8 and 9 shows the velocity and vorticity plots at time $t = 0.5$. Again the translational velocity is well recovered. Also the diffusive vortex movement is well captured. Tables 7 and 8 shows the relative L^2 error and the advection error for various values of α and β.

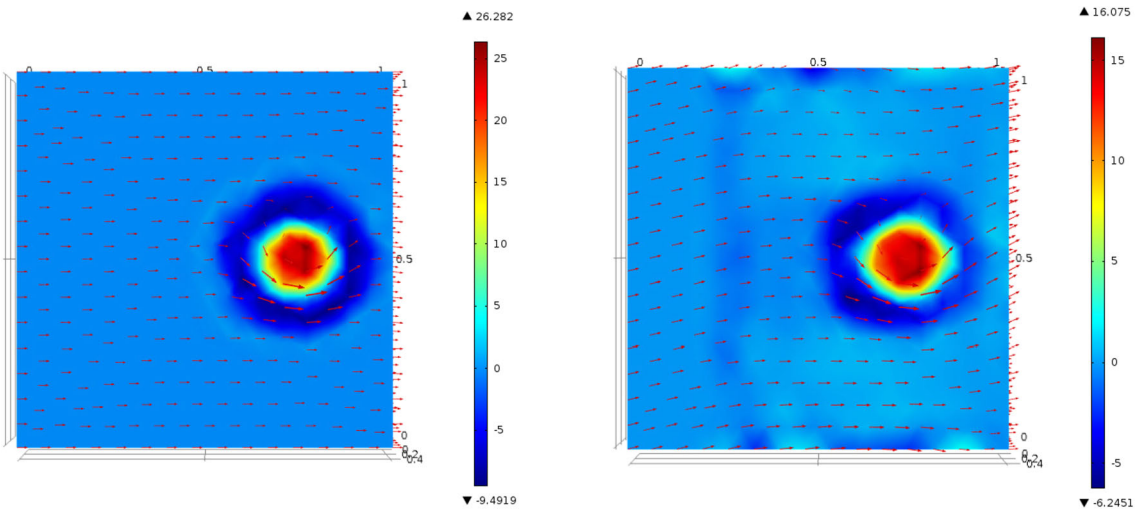

Fig. 10 Velocity and vorticity plots for vortex motion (45) under Euler's flow at $t = 0.5$ for $\alpha = \beta = 1$. **a** Exact, **b** recovered

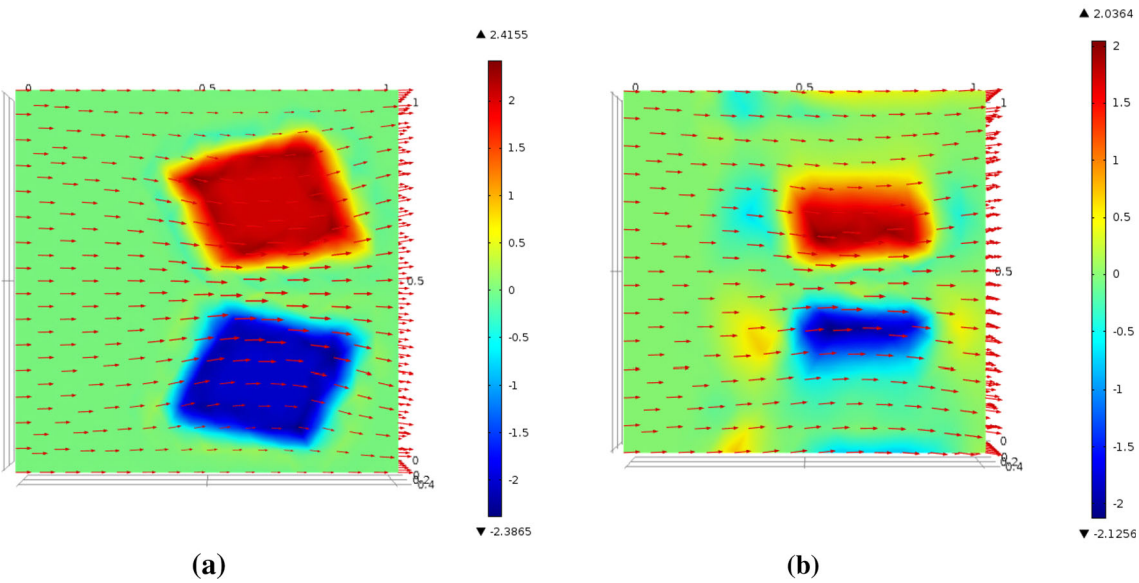

Fig. 11 Velocity and vorticity plots for vortex motion (V2) under Euler's flow at $t = 0.5$ for $\alpha = \beta = 1$. **a** Exact, **b** recovered

8 Formulation 3: Non-linear flow

In this case $\widetilde{\mathbf{U}}$ is determined by minimizing

$$J(\psi(\omega_0,g),\omega_0,g)=\frac{1}{2}\int_Q(E_t+\nabla^\perp\psi.\nabla E)^2 + \frac{\alpha^2}{2}\int_0^T\int_{\partial\Omega}|g|^2+\frac{\beta^2}{2}\int_\Omega|\omega_0|^2 \tag{59}$$

subject to

$$\begin{aligned}\omega_t+\tilde{\mathbf{U}}\cdot\nabla\omega&=0\left(\frac{1}{\mathrm{Re}}\Delta\omega\right),\quad (\mathbf{x},t)\in\Omega\times(0,T]\\ \omega(\mathbf{x},0)&=\omega_0(\mathbf{x}),\quad \mathbf{x}\in\Omega\\ \omega&=0,\quad \mathbf{x}\in\partial\Omega_-(\partial\Omega\text{ for Navier}-\text{Stokes})\end{aligned} \tag{60}$$

$$\begin{aligned}\Delta\psi&=\omega,\quad \text{in }\Omega\\ \frac{\partial\psi}{\partial n}&=g,\quad \text{on }\partial\Omega\end{aligned} \tag{61}$$

$$\begin{aligned}\widetilde{\mathbf{U}}&=\nabla^\perp\psi\\ \omega&=\nabla\times\widetilde{\mathbf{U}}\end{aligned} \tag{62}$$

8.1 Optimization using Lagrange multipliers

We first write down the weak forms of (60) and (61). Multiplying (60) with a test function $y\in H^1([0,T];L^2(\Omega))$, integrating by parts with respect to t and incorporating initial conditions for ω, we get

$$\int_Q(-\omega y_t+(\tilde{\mathbf{U}}\cdot\nabla\omega)y)+\int_\Omega\omega(T)y(T)-\omega_0y(0)=0. \tag{63}$$

If we consider the Navier–Stokes equation then performing an integration by parts over Ω and using boundary conditions on ω, we get

$$\int_Q(-\omega y_t+(\widetilde{\mathbf{U}}\cdot\nabla\omega)y)+\int_\Omega\omega(T)y(T)-\omega_0y(0) +\frac{1}{Re}\int_Q\nabla\omega\cdot\nabla y=0. \tag{64}$$

Multiplying (9) with a test function $\phi\in L^2([0,T];H^1_a(\Omega))$, integrating by parts over Ω, and using boundary conditions on ψ we get

$$\int_Q(\nabla\psi\cdot\nabla\phi-\omega\phi)-\int_0^T\int_{\partial\Omega}g\phi=0. \tag{65}$$

Hence to determine the optimal solution, the auxillary functional can be written as

$$\begin{aligned}&\widetilde{J}(y,\omega,\phi,\psi,g,\omega_0)\\ &=J+\int_Q(-\omega y_t+(\widetilde{\mathbf{U}}\cdot\nabla\omega)y)+\int_\Omega\omega(T)y(T)-\omega_0y(0)\\ &\quad+\int_Q(\nabla\psi\cdot\nabla\phi-\omega\phi)-\int_0^T\int_{\partial\Omega}g\phi\left(+\frac{1}{Re}\int_Q\nabla\omega\cdot\nabla y\right)\end{aligned} \tag{66}$$

where y is the Lagrange multiplier corresponding to the first constraint set (8) and ϕ is the Lagrange multiplier corresponding to the second constraint set (14). Here $\omega,y\in L^2([0,T];L^2(\Omega))$ and $\psi,\phi\in L^2([0,T];H^1_a(\Omega))$ where

$$H^1_a(\Omega)=\left\{\psi\in H^1(\Omega):\int_\Omega\psi=0\right\}$$

8.2 PDE's obtained after minimization of $\widetilde{J}$

Taking the Gateaux derivative of $\widetilde{J}$ in (66) wrt $y,\omega,\phi,\psi,g,\omega_0$, the standard optimality conditions [6] are

$$\frac{\partial\widetilde{J}}{\partial y}=0,\frac{\partial\widetilde{J}}{\partial\omega}=0,\frac{\partial\widetilde{J}}{\partial\phi}=0,\frac{\partial\widetilde{J}}{\partial\psi}=0,\frac{\partial\widetilde{J}}{\partial g}=0,\frac{\partial\widetilde{J}}{\partial\omega_0}=0 \tag{67}$$

The first and second equations in (67) gives the vorticity equation and its adjoint

$$\begin{aligned}&\omega_t+\widetilde{\mathbf{U}}\cdot\nabla\omega=0\left(\frac{1}{Re}\Delta\omega\right)\\ &\omega(\mathbf{x},\mathbf{0})=\omega_{\mathbf{0}}(\mathbf{x})\\ &\omega=0,\quad \mathbf{x}\in\partial\Omega_-(\partial\Omega)\end{aligned} \tag{68}$$

$$\begin{aligned}&y_t+\widetilde{\mathbf{U}}\cdot\nabla y=0\left(-\frac{1}{Re}\Delta y\right)\\ &y(\mathbf{x},T)=0\\ &y=0\quad\text{on }\partial\Omega\end{aligned} \tag{69}$$

The third and fourth equations in (67) gives the equations for the streamfunction and its adjoint

$$\begin{aligned}-\Delta\psi&=\omega,\quad \widetilde{\mathbf{U}}=\nabla^\perp\psi\\ \frac{\partial\psi}{\partial n}&=g\end{aligned} \tag{70}$$

$$\begin{aligned}\Delta\phi&=-\nabla E.\nabla^\perp F\\ \frac{\partial\phi}{\partial n}&=-F\frac{\partial E}{\partial t}\end{aligned} \tag{71}$$

where $F=E_t+\widetilde{\mathbf{U}}\cdot\nabla E$. The fifth and sixth equations in (67) gives the optimality conditions

$$\alpha^2g=\phi,\qquad \beta^2\omega_0=y(0) \tag{72}$$

9 Numerical examples

9.1 Advection of vortex 1 and vortex 2 under Euler's flow

The exact flow is given by solving (43) with initial vorticity given by (45) and (V2) and boundary condition for streamfunction given in Sect. 4.5. Figures 10 and 11 shows the velocity and vorticity plots at time $t=0.5$. Unlike the test cases in Sects. 5.1 and 7.1, we see that the translational

velocity is not well recovered. Also there is a lot of vortex shredding in Fig. 10. It diffuses out the vortex even for Euler's flow. In Fig. 11 we note the vortex patches get diffused to a high extent. Near the red vortex patch there are light blue patches and vice-versa for the blue vortex patch which means vortex shredding takes place. The bad recovery of the vortex patches could be due to lack of non-uniqueness of solution to the vorticity equation (68). Tables 9 and 10 shows the relative L^2 error and the advection error for various values of α and β. As in the test cases in Sect. 5.1, the best results are obtained values of α and β in the range of $[0.1, 10]$.

Table 9 Relative L^2 errors and advection errors for different values of α and β

α	β	Relative L^2 error	Advection error
0.01	0.01	0.21	3.21e−2
0.1	0.01	0.24	3.22e−2
1	1	0.23	3.26e−2

Table 10 Relative L^2 errors and advection errors for different values of α and β

α	β	Relative L^2 error	Advection error
0.01	0.01	0.35	1.64e−2
1	1	0.37	1.62e−2
10	10	0.35	1.61e−2

9.2 Advection of vortex 1 and vortex 2 under Navier–Stokes flow

The exact flow is given by solving (44) with initial vorticity given by (45) and (V2) and boundary condition for streamfunction given in Sect. 4.5. Figures 12 and 13 shows the velocity and vorticity plots at time $t = 0.5$. As in the test cases in Sect. 9.1, we see that the translational velocity and vorticity is not well recovered. There is a lot of vortex shredding and over-diffusivity. Tables 11 and 12 shows the relative L^2 error and the advection error for various values of α and β.

10 Conclusions

To determine vortex based flows, we have assumed they satisfy Euler or Navier–Stokes equations. The vorticity-streamfunction formulation for the Euler and Navier–Stokes equations were introduced and the Helmholtz decomposition of the velocity field was used to segregate the translational and rotational part of the velocity field. To determine the velocity and vorticity field a variational approach to minimize a functional, which penalized the tracking or advection error of the scalar image field and the initial vorticity and boundary condition for the streamfunction, was used. For the linearized case we have shown existence of an unique velocity field. We also exploited the advantages of the discontinuous Galerkin finite elements for the vorticity equation in case of Euler's flow to capture discontinuous vortices effectively. Two types of vortex movement under Euler and

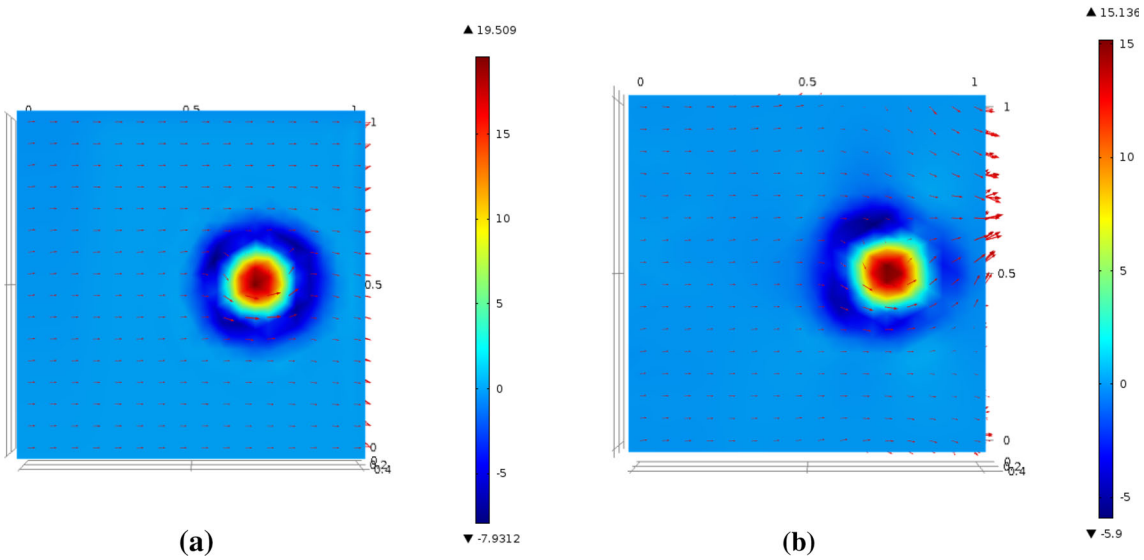

Fig. 12 Velocity and vorticity plots for vortex motion (45) under Navier–Stokes flow at $t = 0.5$ for $\alpha = \beta = 1$. **a** Exact, **b** recovered

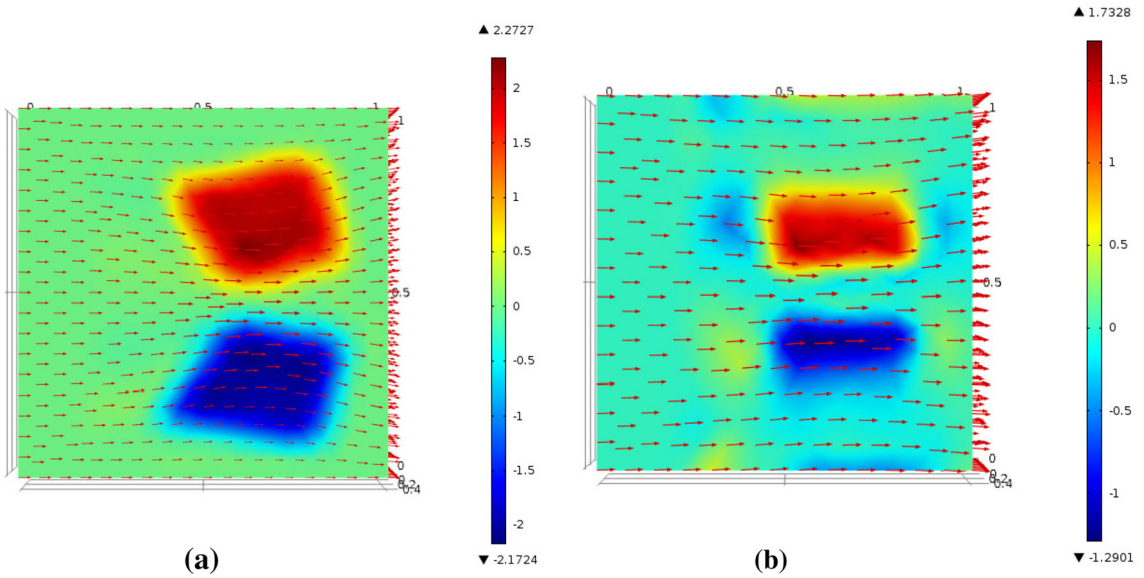

Fig. 13 Velocity and vorticity plots for vortex motion (V2) under Navier–Stokes flow at $t = 0.5$ for $\alpha = \beta = 1$. **a** Exact, **b** recovered

Table 11 Relative L^2 errors and advection errors for different values of α and β

α	β	Relative L^2 error	Advection error
0.01	0.01	0.51	6.6e−2
1	1	0.55	6.1e−2
10	10	0.52	6.7e−2

Table 12 Relative L^2 errors and advection errors for different values of α and β

α	β	Relative L^2 error	Advection error
0.01	0.01	0.60	7.2e−2
1	1	0.64	7.4e−2
10	10	0.65	7.1e−2

Navier–Stokes flows were investigated and it was observed that the results in the cases where we assumed Helmholtz decomposition of the velocity vector field gave significantly good results even for higher Reynolds number flows. In the case where there was no assumption on the velocity field, occurrence of vortex shredding and high diffusion took place. A reason for this could be the non-uniqueness of solutions to the vorticity equation which is itself an interesting theoretical problem. The authors plan to address this in future. It also suggests that to capture vortex structures, boundary information of the velocity or the initial vorticity is needed or else rotational dynamics should be introduced into the model. Further work will be to use other penalties in our objective functional J and try to capture other types of nonlinear flows.

References

1. Horn, B.K.P., Schunck, B.G.: Determining optical flow. Artif. Intell. **17**(1–3), 185–203 (1981)
2. Bauschke, H.H., Combettes, P.L.: Convex analysis and monotone operator theory in Hilbert spaces. In: Dilcher, K., Taylor, K. (eds.) CMS Books in Mathematics. Springer, New York. ISBN: 978-1-4419-9466-0 (2011)
3. Ruhnau, P., Schnörr, C.: Optical Stokes flow: an imaging based control approach. Exp. Fluids **42**, 61–78 (2007)
4. Yuan, J., Ruhnau, P., Mémin, E., Schnörr, C.: Discrete orthogonal decomposition and variational fluid flow estimation. In: Scale-Space 2005, volume 3459 of Lecture Notes Computer Science, pp. 267–278. Springer (2005)
5. Girault, V., Raviart, P.-A.: Finite Element Methods for Navier–Stokes Equations. Theory and Algorithms. Springer Series in Computational Mathematics. Springer, Berlin (1986)
6. Tröltzsch, F.: Optimal Control of Partial Differential Equations: Theory, Methods and Applications. Graduate Studies in Mathematics, vol. 112, American Mathematical Society, USA (2010)
7. Liu, T., Shen, L.: Fluid flow and optical flow. J. Fluid Mech **614**, 253–291 (2008)
8. Heitz, D., Mémin, E., Schnörr, C.: Variational fluid flow measurement from image sequences: synopsis and perspectives. Exp. Fluids **48**, 369–393 (2010)
9. Cayula, J.-F., Cornillon, P.: Cloud detection from a sequence of SST images. Remote Sens. Environ. **55**, 80–88 (1996)
10. Leese, J.A., Novak, C.S., Taylor, V.R.: The determination of cloud pattern motions from geosynchronous satellite image data. Pattern Recognit. **2**, 279–292 (1970)
11. Fogel, S.V.: The estimation of velocity vector-fields from time varying image sequences. CVGIP: Image Underst. **53**, 253–287 (1991)
12. Wu, Q.X.: A correlation-relaxation labeling framework for computing optical flow—template matching from a new perspective. IEEE Trans. Pattern Anal. Mach. Intell. **17**, 843–853 (1995)
13. Parikh, J.A., DaPonte, J.S., Vitale, J.N., Tselioudis, G.: An evolutionary system for recognition and tracking of synoptic scale storm systems. Pattern Recognit. Lett. **20**, 1389–1396 (1999)

14. Logg, A., Mardal, K.-A., Wells, G.N.: Automated Solution of Differential Equations by the Finite Element Method. Springer, Berlin (2012)
15. Hinze, M., Pinnau, R., Ulbrich, M., Ulbrich, S.: Optimization with PDE Constraints. Springer, Netherlands. ISBN 978-1-4020-8839-1 (2009)
16. Aubert, G., Kornprobst, P.: A mathematical study of the relaxed optical flow problem in the space. SIAM J. Math. Anal. **30**(6), 1282–1308 (1999)
17. Aubert, G., Deriche, R., Kornprobst, P.: Computing optical flow via variational techniques. SIAM J. Math. Anal. **60**(1), 156–182 (1999)
18. Nagel, H.-H.: Displacement vectors derived from second-order intensity variations in image sequences. CGIP **21**, 85–117 (1983)
19. Nagel, H.-H.: On the estimation of optical flow: relations between different approaches and some new results. AI **33**, 299–324 (1987)
20. Nagel, H.-H.: On a constraint equation for the estimation of displacement rates in image sequences. IEEE Trans. PAMI **11**, 13–30 (1989)
21. Nagel, H.-H., Enkelmann, W.: An investigation of smoothness constraints for the estimation of displacement vector fields from image sequences. IEEE Trans. PAMI **8**, 565–593 (1986)
22. Papadakis, N., Mémin, E.: Variational assimilation of fluid motion from image sequence. SIAM J. Imaging Sci. **1**(4), 343–363 (2008)
23. Mukawa, N.: Estimation of shape, reflection coefficients and illuminant direction from image sequences. In: ICCV90, pp. 507–512 (1990)
24. Corpetti, T., Mémin, E., Pérez, P.: Dense estimation of fluid flows. IEEE Trans. Pattern Anal. Mach. Intell. **24**(3), 365380 (2002)
25. Nakajima, Y., Inomata, H., Nogawa, H., Sato, Y., Tamura, S., Okazaki, K., Torii, S.: Physics-based flow estimation of fluids. Pattern Recognit. **36**(5), 1203–1212 (2003)
26. Arnaud, E., Mémin, E., Sosa, R., Artana, G.: A fluid motion estimator for schlieren image velocimetry. In: ECCV06, I, pp. 198–210 (2006)
27. Wayne Roberts, A., Varberg, Dale E.: Convex Functions. Academic Press, New York (1973)
28. Haussecker, H.W., Fleet, D.J.: Computing optical flow with physical models of brightness variation. IEEE Trans. Pattern Anal. Mach. Intell. **23**(6), 661–673 (2001)
29. Cockburn, B., Shu, C.-W.: The Runge-Kutta discontinuous Galerkin method for conservation laws V: multidimensional systems. J. Comput. Phys. **141**(2), 199–224 (1998)
30. Cockburn, B., Shu, C.-W.: Runge-Kutta discontinuous Galerkin methods for convection-dominated problems. J. Sci. Comput. **16**(3), 173–261 (2001)
31. Cockburn, B., Karniadakis, G.E., Shu, C.-W.: Discontinuous Galerkin methods. Theory, computation and applications. Lecture Notes in Computational Science and Engineering. Springer, Berlin (2000)
32. Arlotti, L., Banasiak, J., Lods, B.: A new approach to transport equations associated to a regular field: trace results and well-posedness. Mediterr. J. Math. **6**, 367–402 (2009)
33. Blanc, V.L.: L^1-stability of periodic stationary solutions of scalar convection-diffusion equations. J. Differ. Equ. **247**, 1746–1761 (2009)
34. Roy, S.: Reconstruction of a class of fluid flows by variational methods and inversion of integral transforms in tomography, Ph.D. dissertation, Tata Institute of Fundamental Research, CAM, Bangalore. https://www.dropbox.com/s/cbxblk3dg7kwxp5/Souvik_phd_thesis_compressed.pdf?dl=0 (2015)
35. Roy, S., Chandrashekar, P., Vasudeva Murthy, A.S.: A variational approach to optical flow estimation of incompressible fluid flow. J. Comput. Vis. Sci. (2015, submitted)